

A Multichannel Electrochemical Sensor Interface IC for Bioreactor Monitoring

Qiuyang Lin, *Member, IEEE*, Wim Sijbers, Christina Avdikou, Didac Gomez, *Member, IEEE*,
Dwaipayyan Biswas, Bernardo Tacca, Nick Van Helleputte, *Member, IEEE*

Abstract—This research paper introduces a novel integrated circuit (IC) designed for bioreactor applications catering to multichannel electrochemical sensing. The proposed IC comprises 2x potentiometric, 2x potentiostat, 2x ISFET channels and 1x temperature conveyor-based architecture with a programmable mirroring ratio, enabling an extensive measurement range of 114 dB. The potentiometric channel incorporates a customized electrostatic discharge (ESD) protection circuit to achieve ultra-low input leakage in the picoampere range, while the ISFET channel employs a constant-voltage, constant-current topology for accurate pH measurement. Combined with the die temperature sensor, this IC is well-suited for monitoring bioreactions in real-time. Additionally, all channels can be time-multiplexed to a reconfigurable analog backend, facilitating the conversion of input signals into digital codes. The prototype of the IC is fabricated using 0.18 μm standard CMOS technology, and each channel is experimentally characterized. The interface IC demonstrates a peak power consumption of 22 μW .

Index Terms— Potentiostat, potentiometry, ISFET, current conveyor, dynamic range (DR), low leakage, ESD protection, pH measurement, electrochemical, bioreactor, low-power.

I. INTRODUCTION

BIOREACTORS have become integral in various aspects of our daily lives, serving as systems or devices that create and maintain biologically active environments [1]. Their applications span across many industries, such as food, pharmaceuticals, and research activities (Fig.1). For instance, for the production of beer, yogurt, and cheese in the brewery and dairy industry, yeast and lactic acid bacteria (LAC) are responsible for the fermentation process, wherein essential bio/chemical reactions take place within the bioreactor. Monitoring these reactions in real-time with precise measurements of key chemical parameters like temperature, dissolved oxygen (DO), pH, and glucose level is critical for these enzyme/bacteria-related reactions. To achieve this, an electrochemical sensor interface is formed by integrating sensors/electrodes/transducers and a readout integrated circuit (IC) [2].

Among the various sensing mechanisms, potentiometry and amperometry play significant roles. A redox reaction involves oxidation and reduction at the working electrode (WE) and reference electrode (RE), respectively [2][3]. This results in a



Fig. 1 Bioreactor applications for industry and research purposes.

potential difference proportional to the concentration of the analyte between the two electrodes, known as potentiometric measurement. Moreover, amperometry can measure the redox current. To avoid unwanted IR drop over the RE electrode, the reaction current can be provided via a chemically inert counter electrode (CE). This results in a well-known 3-terminal electrochemical cell which requires a potentiostat circuit for proper voltage biasing and current sensing current. The Faradaic currents are then generated by electron exchange during the redox reaction [5][6]. pH measurement can be achieved using an ion-selective field-effect transistor (ISFET), where the pH value alters the ISFET threshold voltage [7][8], subsequently affecting the gate-source voltage. These chemical

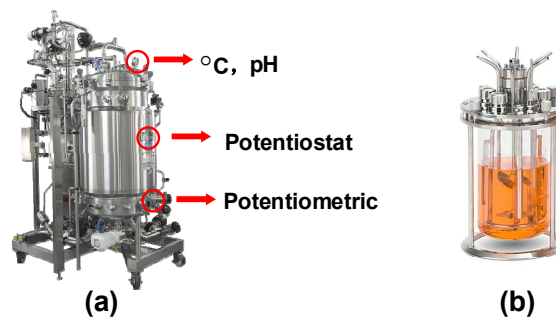


Fig. 2 (a) Big tank bioreactor for industrial use. (b) Small bioreactor vessel/tube for vaccine, pharmaceutical development, and other research purpose.

Manuscript received XX, XX; revised XX and XX; accepted XX.
(Corresponding Author: Qiuyang Lin, Qiuyang.lin@imec.be)

Q. Lin, W. Sijbers, C. Avdikou, D. Biswas, B. Tacca and N. Van Helleputte are with the imec, Heverlee, 3001, Belgium.

D. Gomez was with imec, Heverlee 3001, Belgium, now with MPS Spain, Barcelona, Spain.

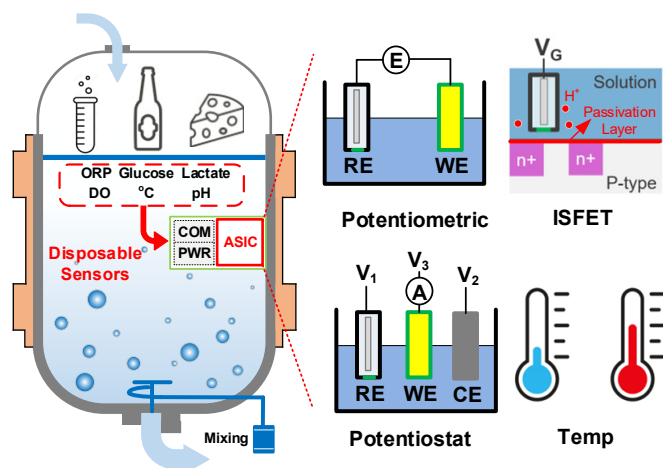


Fig. 3 The vision of the proposed electrochemical interface IC in bioreactor monitoring tasks and the potential measurement modalities.

parameters can be converted into voltage or current signals and digitally read out using an interface IC, enabling precise control over reactions, improved productivity, and avoidance of undesired byproducts.

The size of bioreactors ranges from large tanks used in manufacturing and industrial applications to smaller vessels or tubes (Fig. 2) utilized for research purposes like vaccine development or medical testing [9][10]. In conventional setups, electrochemical sensing modules are typically placed on the surface of the tank, where each sensing channel can be an individual meter or machine due to the ample surface area available. These channels can be powered by the mains power source through cables. However, when it comes to bioreactors in the form of vessels and tubes, replicating the same approach becomes challenging due to limited form factor constraints. Another significant concern is the rapid degradation of sensors/electrodes commonly observed in electrochemical applications [11], necessitating frequent replacement or calibration, which is not user-friendly. Recent advancements in integrated circuit technology provide an opportunity to address these issues more effectively. To overcome the aforementioned challenges, our objective is to develop a compact, low-power interface IC with multimodal electrochemical sensing capabilities, including potentiometric, potentiostat, ISFET, and temperature channels (Fig. 3). Along with a separate power module and wireless communication block, this IC can be integrated seamlessly with disposable sensors. Consequently, all monitoring tasks can be easily accomplished by simply introducing the system into the solution, suiting small bioreactor vessel requirements. This paper focuses solely on the sensor interface IC, which finds frequent usage in cutting-edge bioreactor sensing applications [12][13]. However, challenges still persist for each individual sensing channel.

Amperometry is a standard method to measure redox reactions [2][14]. Therefore, it is crucial to incorporate bidirectional current measurement capability, as oxidation and reduction reactions typically exhibit opposite current directions [15]. As mentioned before, a typical electrochemical cell has a working electrode (WE) where the reaction takes place, a reference electrode (RE), and a counter electrode (CE)

electrode. The potentiostat circuit has to provide a well-defined voltage difference between RE and WE to maintain the desired reaction while simultaneously measuring the reaction current. Typically, no current should flow into the RE electrode. Instead, a CE completes the circuit and provides the current flowing out of the WE. [16]. The voltage biasing and expected redox current depend greatly on the specific redox reaction one wants to monitor. Hence the potentiostat circuit must support a wide measurement range, capable of accommodating currents ranging from picoamperes to microamperes [17]-[19]. Secondly, potentiometric measurements are employed to determine the concentration of a solute in a solution. It involves measuring the potential between the RE and the ion-selective electrode (ISE) or working electrode [20][21]. Since solute concentrations can be extremely low and potentiometric measurements are typically valid in electrochemical equilibrium only, the interface IC must exhibit a very high input impedance ($>G\Omega$) to accurately capture the potential and avoid stray current flow which would perturb equilibrium. In pH monitoring, a CMOS passivation layer is sensitive to hydrogen ions or other target ions if a selective membrane is deposited. Consequently, the overdrive voltage of the ISFET changes accordingly (Fig. 3) [22]. However, it should be noted that within the liquid gate, trapped charges can lead to undesired DC shifts. Therefore, the readout circuit requires a large input compliance range and programmability in terms of current and voltage biasing [23].

We propose a multimodal electrochemical sensing integrated circuit (IC) that addresses the requirements of a compact form factor and low power consumption. The prototype of this IC is implemented using standard $0.18\ \mu\text{m}$ CMOS technology. It incorporates two potentiometric channels, two potentiostat channels, two ISFET channels, and a temperature channel, enabling comprehensive sensing capabilities for bioreactor applications. The potentiostat channel employs a programmable current conveyor architecture, facilitating bidirectional current measurement with an exceptional range of 114 dB. To achieve high-performance potentiometric measurements, the potentiometric channel incorporates a custom electrostatic discharge (ESD) protection circuit that ensures an input impedance greater than $350\ G\Omega$ and a leakage current of less than $2.5\ \text{pA}$. The ISFET channel, coupled with the readout circuitry, delivers a wide programmable biasing range, ensuring excellent linearity and signal-to-noise ratio (SNR). To seamlessly integrate the frontend channels, a time-multiplexing switch matrix, and efficient analog backend are designed, resulting in a low power consumption of $< 22\ \mu\text{W}$.

This paper is an extended version of [24], and the rest of the paper is organized as follows. Section II describes the system architecture and the operating principles of the interface IC. Section III shows the detailed circuit implementation of each channel. Section IV describes the electrical and in-vitro measurement results, while section V draws the conclusion.

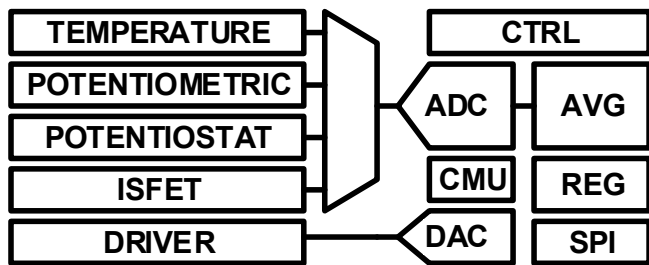


Fig. 4 The simplified system diagram.

II. THE PROPOSED ARCHITECTURE

The system architecture of the interface IC is described in this section, including the block diagrams. Moreover, details about the reconfigurable analog backend are introduced.

A. Motivation and system architecture

Previous works on electrochemical sensing ICs have primarily focused on single-modality sensing approaches, such as using a single potentiostat channel for glucose monitoring [25][26] or ISFET channels for pH sensing and imaging [27][28]. However, the bioreactor environment is often more complex, requiring the measurement of parameters like dissolved oxygen (DO), concentration, and temperature, which are crucial for enzymes and other reactions. To address this need, a multifunctional chip with different channels is proposed. Existing electrochemical chips cannot measure as many modalities in a sufficiently power-efficient manner [29][31]. A simplified system diagram is presented in Fig. 4, where all readout channels are implemented on the same IC, and the analog input signals are converted to digital codes by an ADC. Digital control, register, and clock management unit (CMU) are included. The IC communicates with the microcontroller through an SPI module.

The detailed block diagram is shown in Fig. 5. Two

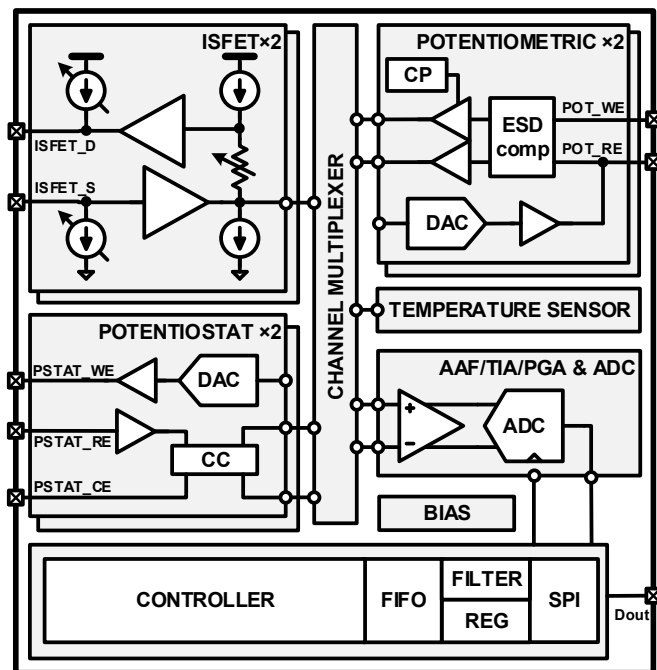


Fig. 5 (a) The detailed circuitry blocks of electrochemical interface IC.

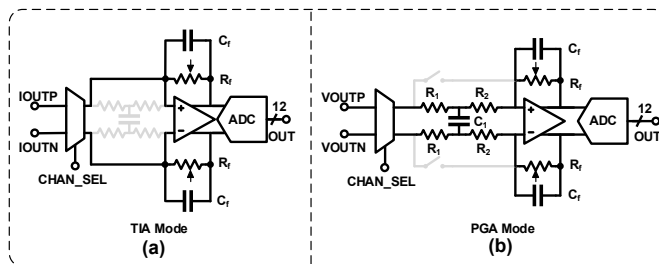


Fig. 6 The reconfigurable analog backend: (a) TIA mode for current readout; (b) PGA mode for voltage readout.

potentiostat channels are implemented, each equipped with an on-chip buffer to provide a voltage bias to the WE. The voltage applied to the WE can be digitally controlled using a DAC with a full voltage range spanning from the ground to the supply voltage. The RE voltage is regulated to the reference voltage (set to mid-supply) using a buffer and a negative feedback loop. The bidirectional current from the CE is sensed with a current conveyer completing the potentiostat circuit which is further explained in section III. A (see also Fig. 7). Two potentiometric channels are implemented, where the RE can be biased using a buffer that can be adjusted as needed. The voltage difference between WE and RE is sensed through two pseudo-differential buffers. To minimize input bias current, ESD compensation is applied. Moreover, two ISFET channels are implemented using the constant-current, constant-voltage architecture. The bias current and drain-source voltages of the ISFET are programmable. A die temperature sensor is employed to monitor the temperature in real-time (-40°C to 70°C , equivalent measured readout noise $< 0.05^{\circ}\text{C}$) with a conventional bipolar implementation [30]. All channels are time-multiplexed to a switch matrix. The analog backend is responsible for filtering, amplification, and A-to-D conversion. The digital control includes setting registers, clock control, digital filters, and a communication module. This architecture is suitable for multimodal electrochemical monitoring, especially for bioreactor applications, as described in the previous chapter.

B. Reconfigurable analog backend

The analog front end of the interface IC performs the conversion of all electrochemical signals into either current or voltage signals prior to the channel multiplexer. However, to accommodate the different signal amplitudes and bandwidths, the analog backend requires optimization in terms of amplification and filtering before transmitting the signals to the ADC. A reconfigurable and fully differential analog backend is designed to integrate with all the channels.

In the potentiostat channel, the output signal is in the form of a current due to the use of a current conveyer. The trans-impedance amplifier (TIA) mode is employed to amplify this current signal. The trans-impedance gain is determined by the feedback resistor (R_f), which can be programmed and set within a range of $4\text{ M}\Omega$ to $40\text{ M}\Omega$ (Fig. 6 (a)). R_f is in parallel with C_f , which sets the low-pass corner for the TIA, serving as an anti-aliasing filter (AAF) and eliminating out-of-band noise prior to the A-D conversion. Similarly, for voltage output signals, the analog backend is reconfigured to operate in the programmable gain amplifier (PGA) mode (Fig. 6 (b)). The feedback resistor

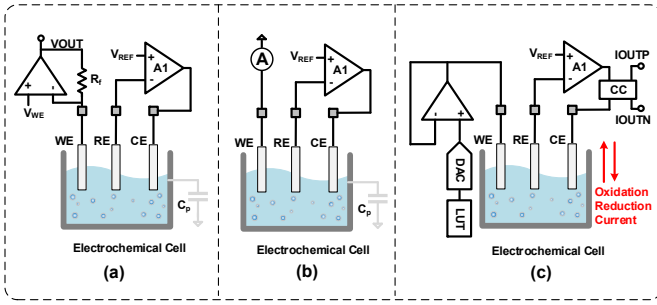


Fig. 7 (a) Conventional potentiostat topology. (b) Conventional potentiostat with RE shorted to ground or supply. (c) Proposed current conveyor based potentiostat.

R_f and $(R_1 + R_2)$ set the voltage gain. R_1 , together with C_1 set the low-pass corner to behave like AAF. The value of R_1 is $5\text{ M}\Omega$ and C_1 is programmable up to 4 pF . This reconfigurable analog backend is shared among all channels, enabling the conversion of analog signals into digital codes while conserving power and chip area. The ADC is also shared between all channels. It is a SAR-based ADC running 32 kS/s with 12 bits resolution.

III. CIRCUIT IMPLEMENTATION

This section provides a detailed description of each channel's implementation and circuit blocks, including the potentiostat channel current conveyor, potentiometric channel ESD compensation circuit, and ISFET channel circuit. The motivations and design considerations behind each circuit block are also elucidated.

A. The potentiostat and current conveyor

Fig. 7 (a) shows a typical electrochemical measurement by a potentiostat. The two amplifiers will maintain a voltage difference between the RE and WE (equal to $V_{WE} - V_{REF}$). A (chemically inert) CE electrode is used to provide the reaction current since no current should flow in the RE. A TIA will generate an output voltage proportional to the redox current I_{ion} , R_f is the feedback resistor:

$$V_{out} = I_{ion}R_f \quad (1)$$

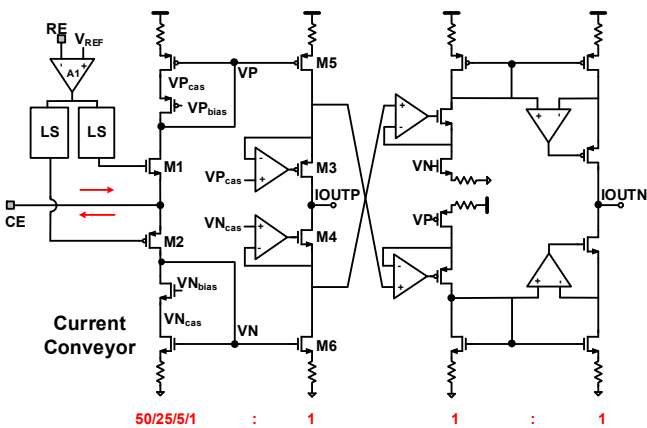


Fig. 8 Schematic of the bidirectional current conveyor with programmable gain and fully differential output.

However, this configuration introduces an extra pole and decreases the stability of the potentiostat due to the unknown parasitic capacitance between the WE and the electrochemical cell [3][26]. One conventional solution is to short the WE to ground (or the supply) and measure the current flowing through the WE (Fig. 7 (b)). However, this approach usually only allows sensing of the ion current in one direction (sink when WE is grounded, source when it is connected to supply), which is not ideal [16][17]. Instead, the proposed method uses the WE solely for voltage biasing, while the reaction current is sensed in the CE. Since no current should flow into the RE, the reaction current flows from CE to WE and can hence be measured in either electrode. Since the CE is connected to a low-impedance node (the output of a buffer), stability issues are mitigated. By biasing the RE at mid-supply and allowing the WE voltage to have a rail-to-rail swing, the proposed topology supports bidirectional redox current (Fig. 7 (c)). This current is then mirrored into a current conveyor (CC).

The circuit implementation of the current conveyor is presented in Fig. 8. In order to sense bidirectional current, the current conveyor must be capable of sourcing and sinking full-range current with a low input impedance. Thus, CE is connected to the source of M_1 and M_2 . To regulate the RE voltage, RE and CE are connected in a negative feedback scheme. The output of amplifier A_1 is connected to two level shifters to ensure that both M_1 and M_2 are active. Depending on

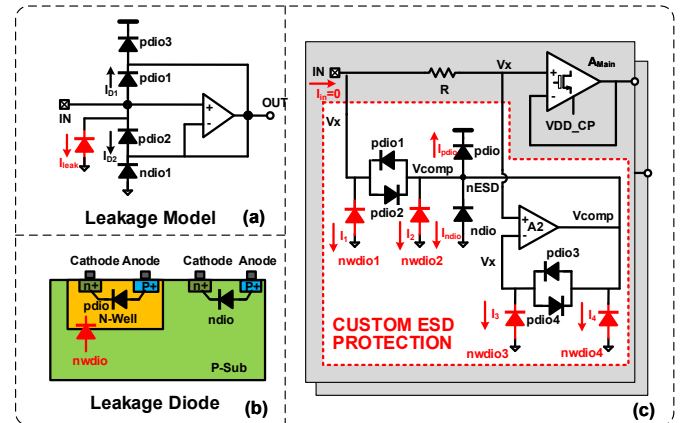


Fig. 9 (a) Conventional ESD compensation method. (b) The parasitic diode and the leakage model of the conventional ESD compensation. (c) The proposed custom ESD protection.

the direction of the current, either a PMOS or NMOS current mirror is enabled to copy the current to the output branch. Different from other conventional CC architectures [32][33], this circuit ensures constant drain-source voltages of the mirroring transistors to improve current mirroring accuracy and to avoid the channel modulation effect. Regulating circuits, consisting of transistors M_3 and M_4 , are built to fix the drain voltage of M_5 and M_6 to $V_{P_{cas}}$ and $V_{N_{cas}}$, respectively. These regulating circuits also help reduce the noise of M_3 and M_4 . A source degeneration circuit is used to further minimize the mirroring transistors' noise and improve the current mirror's linearity. To expand the measurement range of the potentiostat, the input branch can be programmed with a 50:1 ratio with respect to the output branch, supporting a total input current range of $\pm 200\text{ nA}$ to $\pm 10\text{ }\mu\text{A}$. Additionally, a single-to-differential topology is employed to integrate with the analog

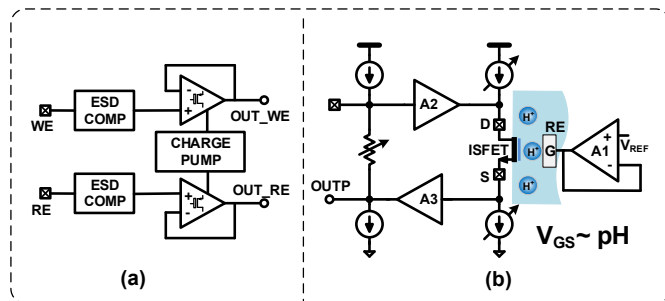


Fig. 10 (a) Pseudo-differential potentiometric channel with thick oxide input pair. (b) Constant-current constant-voltage ISFET channel.

backend in a fully differential trans-impedance amplifier (TIA) mode. However, it should be noted that the single-to-differential architecture may not improve the signal-to-noise ratio (SNR) as it introduces more noise contributors and may introduce even-order harmonics during mirroring.

B. The potentiometric channel and custom ESD

Maintaining a low leakage current at the potentiometric interface is crucial for preserving chemical equilibrium. ESD can introduce significant leakage, reaching nA or even μA levels, particularly at elevated temperatures common in bioreactor applications. Conventional ESD compensation methods, as shown in Fig. 9 (a), utilize diodes $p_{\text{dio}1}$ and $p_{\text{dio}2}$ in a reverse-biased configuration with identical sizes and using a regulation loop to equalize the biasing voltages. Thus, the leakage currents through these diodes cancel each other out. A similar principle can be applied to $p_{\text{dio}3}$ and $n_{\text{dio}1}$ to further nullify leakage currents. However, the introduction of $p_{\text{dio}2}$ comes with an additional parasitic diode from N_{well} to P_{sub} which might exhibit leakage (Fig. 9 (a)), potentially degrading the performance of the interface IC in applications demanding ultra-low leakage [34]. Hence, we implement a custom ESD protection with improved leakage compensation (Fig. 9 (c)). The input (IN) is ESD protected with anti-parallel diodes $p_{\text{dio}1,2}$ to an intermediate net (nESD) which itself is protected with standard ESD protection [35]. $p_{\text{dio}3,4}$ are replicas of $p_{\text{dio}1,2}$ and, thanks to amplifier A_2 , are similarly biased, hence exhibiting the same leakage current. The feedback loop of A_2 will ensure that the voltage $V_x = V_{\text{in}}$. Since no current can flow from the negative terminal of A_2 , A_2 will find a voltage V_{comp} such that all the leakage current will be provided by the amplifier. Since this bias condition is copied to the actual input, it follows that I_{in} should be 0. In reality, the input impedance will be limited

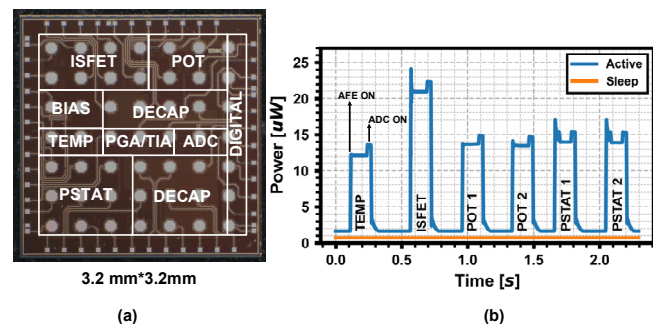


Fig. 11 (a) Die micrograph of the 3.2x3.2mm² chip fabricated in TSMC 0.18 μm with visible flip-chip bumping pads. (b) Power breakdown of all channels, peak power is founded when ISFET channel enabled.

only by mismatch and finite open-loop gain of A_2 . The same technique is applied to the potentiostat channels.

Besides using a custom ESD protection circuit, the input pair of the main amplifier A_{main} applies a thick-oxide transistor, further decreasing the leakage current. A pseudo-differential topology is used to buffer both voltages from the WE and RE, where both buffers are supplied by a 3.6 V voltage generated by an on-chip charge pump (Fig. 10 (a)). This configuration enables the potentiometric channel to have higher voltage headroom while maintaining high linearity.

C. ISFET channel

The ISFET and its readout circuit form the ISFET channel, which is used to measure the solution's pH. Fig. 10 (b) shows the circuit implementation of the ISFET channel. An on-chip buffer is utilized to bias the liquid gate at a desired voltage. The pH value, which corresponds to the concentration of hydrogen ions, can influence the threshold voltage of the ISFET. Thus, the pH values can be determined by measuring the gate-source

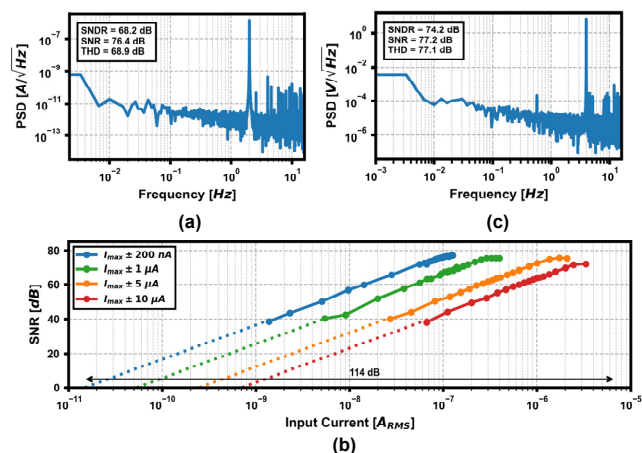


Fig. 12 (a) Potentiostat output spectrum with 176nA, 2Hz sine current input. (b) Potentiostat SNR vs. I_{in} with 4 input range settings and maximum measurement range. (c) Potentiometric channel output spectrum with 1.4 V_{pp}, 4 Hz sinewave voltage input.

voltage of the ISFET. The constant-voltage, constant-current topology is used [37], where the drain voltage is a level-shifted copy of the source voltage, provided by flowing a current through a programmable resistor. The drain-source current is set by two current sources/sinks, where the ISFET is now working in a common drain configuration. The source voltage is buffered to the output. The drain-source current of the ISFET can be adjustable and ranges from 10 nA to 100 μA . The drain-source voltage biasing can also be programmed from 25 mV to

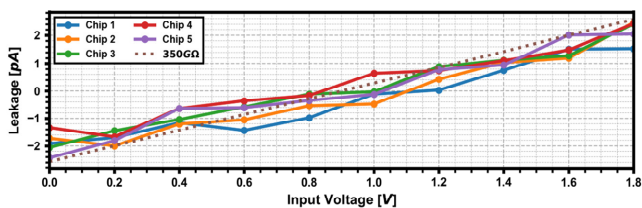


Fig. 13 A measurement demonstrates the effectiveness of the custom ESD protection input leakage compensation. We measured 5 samples across the whole input voltage range. The leakage remains below 2.5pA and is limited by parasitics in our measurement setup.

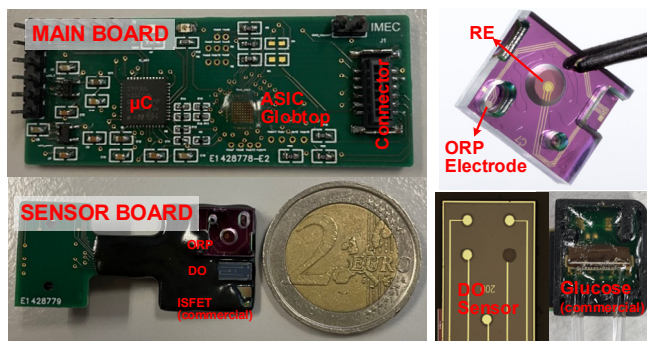


Fig. 14 Initial proof-of-concept board for bioreactor monitoring and the related sensors including DO sensor, commercial ISFET, commercial glucose sensor and ORP electrode.

600 mV. This design approach enables compliance with a multitude of potential ISFET sensors.

IV. MEASUREMENT RESULTS

This electrochemical interface IC has been implemented and fabricated in a standard TSMC 0.18 μm CMOS technology. Fig. 11 (a) shows the micrograph of the prototype, occupying a total area of 10.24 mm^2 . The majority of the chip area is dedicated to analog blocks, with all digital control functions, such as low-level timing, clocking, and digital filters, occupying a minor part of the area. The communication protocol between the chip and PC follows the standard SPI interface. The readout IC operates from a supply voltage of 1.8 V, and the power consumption breakdown for each channel is presented in Fig. 11 (b). The ASIC can be operated in a time-multiplexed manner. Most channels consume $<15\mu\text{W}$, while the ISFET channel consumes $22\mu\text{W}$. Since electrochemical measurement typically only need to happen sporadically, the ASIC offer a low standby power of around $0.7\mu\text{W}$. The on- and off-times in fig. 11 b are merely indicative. In any real scenario, they should match the expected settling time of the sensor. The bumping pads on the IC offer the potential for 3D packaging or chiplet integration, providing flexibility in packaging.

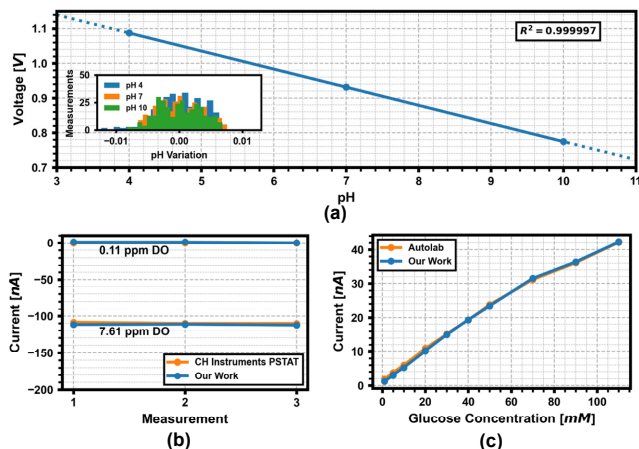


Fig. 15 (a) ISFET channel pH measurement with a commercial ISFET in buffer solutions & pH measurement variance (inset). (b) Dissolved Oxygen two-point measurement vs. commercial setup (bottom-left) with PSTAT channel. (c) Glucose measurement with commercial sensor using PSTAT channel vs. commercial readout (bottom-right). DO/glucose measurement are averaged 1-second-long/30-second-long recording sampled at 32 Sps (In total 960 samples).

For electrical performance characterization we used standard equivalent RC impedance models for electrochemical cells to account for electrode-loading where appropriate. For the potentiostat channel, a voltage sine-wave signal from the signal generator was connected to the CE through resistors ranging from 4 MOhm to 80 kOhm, resulting in an input current ranging from ± 200 nA to ± 10 μA . Fig. 12 (a) shows the recorded output spectrum for a 176 nA, 2 Hz input sinewave current. The ADC is running at 32 kHz, and the digital data output is decimated with a factor of 1024. Therefore, the final output data rate is 32 S/s. As can be seen from the spectrum, an SNR of 76.4 dB and SNDR of 68.2 dB are obtained, equivalent to an ENOB of 11 bits. The main nonideality is distortion, as the spectrum only shows a THD (Total Harmonic Distortion) of 68.9 dB. It confirms the dominant contributors to distortion are the even-order harmonics introduced by the single-to-differential topology. Additionally, since the data rate of this design is 32 Sps, it has the potential to down-convert mains interference (50 Hz) to the baseband frequency. We could also calculate the total integrated noise from those spectra, which is around 14pArms.

Using the same setup, we measured the SN(D)R for various input amplitudes (see Fig. 12(b)). The chip supports 4 different gain settings to cover a wide dynamic range. In the highest gain setting, the input-referred noise is around 14pArms, and the maximum input signal is ± 200 nA, which can be increased with different gain settings all the way up to $\pm 10\mu\text{A}$ spanning a 114dB dynamic range.

To assess the performance of the potentiometric channel, a 1.4 Vpp, 4 Hz sinewave voltage was applied and measured (Fig. 12(c)). The results reveal an SNR of 77.2 dB and an SNDR of 74.2 dB for the potentiometric channel. These values indicate that both noise and distortion play equally significant roles in the nonidealities of the channel. The presence of mains interference and flicker noise is noticeable but does not degrade SN(D)R significantly.

Besides the noise performance, the characterization of the custom ESD block's input leakage current and the potentiometric channel's input impedance holds significant importance. To evaluate these parameters, the potentiometric channel was activated, and its input was connected to a source meter (Keysight B2962A). The input voltage was swept from the ground to the supply voltage while measuring the input current (Fig. 13). The measured input leakage of the potentiometric channel over the entire 1.8V input range remains below 2.5pA (limited by parasitics in the measurement setup). This corresponds to an equivalent input resistance ($\Delta V/\Delta I$) of over 350 G Ω . In total, five chips have been measured to confirm the robustness of the custom ESD circuit.

The electrochemical interface IC is also validated in an in-vitro environment, mimicking real bioreactor measurements. The main PCB contains the electrochemical sensor interface IC and a microcontroller to stream the data to a PC. Various sensor PCBs can be plugged into the main PCB. One example of such a sensor PCB with our electrochemical reference electrode, oxidation-reduction potential (ORP) electrode, DO electrode, and commercial ISFET/glucose devices is also shown. We chose an off-chip ISFET instead of an on-chip one because it

TABLE I PERFORMANCE COMPARISON

	This work	[38] ISSCC'22	[39] ISSCC'20	[40] ISSCC'19	[41] CICC'18	[31] AD5940	[42] ISSCC'21
Applications	Bioreactor	Bio-Sensing	Drugs	DNA	Alcohol	Chemical	Wound
Technology	0.18 μm	0.18 μm	65 nm	0.25 μm	65 nm	--	0.18 μm
VDD	1.8 V	1.8-2.2 V	--	5 V	0.9 V	2.8-3.6 V	1.2 V
Area	10.24 mm ²	23.31 mm ²	0.385 mm ²	63 mm ²	1.275 mm ²	15.12 mm ² ^d	8 mm ²
Total Power	22 μW (peak)	58 mW ^a	220 μW ^b	250 μW	0.97 μW	4.55 mW ^c	49 μW
TEMP	Yes	No	No	No	No	Yes	Yes
Potentiometric	Yes	No	No	No	No	Yes	No
Max. Leakage	2.5 pA	--	--	--	--	20 pA	--
Input Range	1.8 V	--	--	--	--	1.82 V	--
Noise	72.3 μV_{rms}	--	--	--	--	24 μV_{rms} ^f	--
Bandwidth	16 Hz	--	--	--	--	450 Hz	--
ISFET	Yes	No	No	No	Yes	No	No
Noise	6 mpH _{rms}	--	--	--	6.6 mpH _{rms} [*]	--	--
pH Range	4-10	--	--	--	6.8-7.4	--	--
Potentiostat	Yes	Yes	Yes	Yes ^e	Yes	Yes	Yes
Noise	14 pA _{rms}	39 fA _{rms}	15.2 pA _{rms}	0.28 pA _{rms}	1.24 nA _{rms}	--	2 pA _{rms}
Bandwidth	16 Hz	--	5 Hz	20 Hz	--	--	1-1000 Hz
Max. Input	$\pm 10 \mu\text{A}$	300 pA	$\pm 0.8 \mu\text{A}$	$\pm 12.5 \text{nA}$	80 nA	$\pm 750 \mu\text{A}$ ^g	$\pm 6.14 \mu\text{A}$
Max. Range	114 dB	78 dB	100 dB	93 dB	30.2 dB	--	129.7 dB

^a Including pixel power & circuit ^b 5.25 mW before duty-cycling ^c External Potentiostat ^d Wafer Level Chip Scale Package ^e Analog peripheral in idle mode and ADC ^f ADC noise only for PGA gain of 1 and 900Hz update rate ^g Low-power mode ^{*} Calculated from the graphs

has high sensitivity [36]. In our proof-of-concept, only the sensor board is waterproofed by simply covering all the exposed connections with epoxy. Fig. 14 provides a detailed close-up view of some of the sensors employed for the validation of the interface IC.

The ISFET channel is first validated by pH measurement. The ISFET is dipped into three buffer solutions with different pH values (pH 4, 7, and 10). The RE voltage is fixed to 1.6 V, and Fig. 15 (a) shows the source voltage of the ISFET, confirming the 52 mV/pH sensitivity as expected for this ISFET device. It also achieves an R^2 of 0.99999. Multiple measurements have been done to measure the noise of the ISFET channel. The inset figure shows the standard deviation of the individual recordings. The input-referred ISFET channel plus sensor noise is 0.006 pH_{rms}.

Then, the potentiostat channel is validated by DO and glucose measurements. Fig. 15 (b) also shows an amperometric recording of a Pt microelectrode, functionalized for DO measurement. A beaker of water is first pumped by nitrogen to drive out all the DO, which is then measured at 0.11ppm by a commercial DO meter (CH instruments potentiostat). Another sample beaker of water is at room temperature, and the measured DO is 7.61 ppm. These samples were then measured using the interface IC. Each data point shown in Fig. 15 (b) was obtained by measuring at 32Sps during a 1s period and calculating the average. Fig. 15 (c) shows the results of a simple glucose titration experiment using a commercial off-the-shelf-glucose sensor. For this experiment, we measured each concentration value for 30s (again sampled at 32Sps) after

allowing the mixture to settle and calculated the average value obtained. We repeated the protocol with Autolab, which yielded very similar results. For completeness, the standard deviation of these glucose measurements was around 2nA_{rms}, which is completely dominated by the sensor/environmental noise.

In the experimental setup depicted in Fig. 16(a), one of the sensor boards was mounted on the main board and immersed in a test solution to perform an ORP measurement with the potentiometric channel. Five ORP measurements were recorded

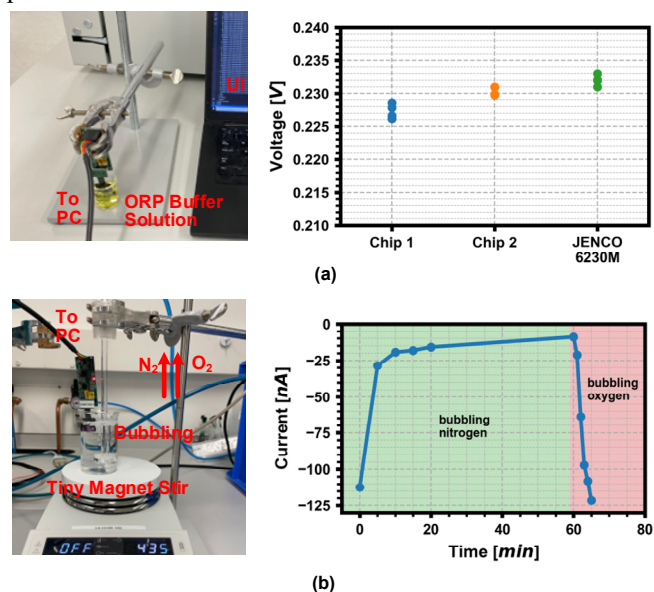


Fig. 16 (a) ORP measurement with the potentiometric channel. (b) Dynamic DO measurement with potentiostat channel.

with two different ASICs, and the results (without sensor calibration) were compared to a commercial Jenco potentiometer. To evaluate the potentiostat's performance in a dynamic environment, another experiment was conducted using DO electrodes, as shown in Fig. 16(b). The sensor board with the electrodes was immersed in a water solution. Initially, pure nitrogen was bubbled into the solution for an hour, effectively removing all dissolved oxygen. This process is clearly observed in the recorded curve, where the current experiences a significant drop, approaching 0. Subsequently, oxygen was bubbled through the solution, leading to rapid dissolution and generating a prompt recovery response.

Table I provides a comprehensive summary of the performance characteristics of the proposed interface IC, accompanied by a comparison to recently published electrochemical interface ICs. The chip achieves a maximum measurement range of 114 dB with a potentiostat channel, a <2.5 pA leakage, and >350 G Ω impedance with a potentiometric channel. The ISFET channel has five digits R^2 and 6 mpH_{rms} noise. Meanwhile, a low peak power consumption of 22 μ W is reported.

V. CONCLUSION

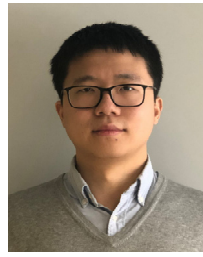
This paper presents a low μ W range electrochemical interface IC for bioreactor applications. The proposed readout architecture achieves a high current measurement range in the potentiostat channel, low leakage, and high input impedance in the potentiometric channel. The ISFET channel achieves low noise and high linearity. This chip is capable of comprehensive bio/chemical tasks, and measures die temperature while only consuming 22 μ W peak power. The IC has been validated with in-vitro DO, glucose, pH, and ORP measurements and compared to reference systems, showing high accuracy and robustness. These results highlight the potential of this interface IC to enable the development of compact, power-efficient, and high-performance monitoring systems for both industrial bioreactors and research-based miniature bioreactors.

REFERENCES

- [1] McNaught, Alan D. *Compendium of chemical terminology*. Vol. 1669. Oxford: Blackwell Science, 1997.
- [2] Y. Ma *et al.*, "A Review of Electrochemical Electrodes and Readout Interface Designs for Biosensors," *IEEE Open Journal of the Solid-State Circuits Society*, Vol. 3, pp. 76-88, 2023.
- [3] Bard, Allen J., Larry R. Faulkner, and Henry S. White. *Electrochemical methods: fundamentals and applications*. John Wiley & Sons, 2022.
- [4] S. -Y. Lu *et al.*, "A Review of CMOS Electrochemical Readout Interface Designs for Biomedical Assays," *IEEE Sensors Journal*, Vol. 21, no. 11, pp. 12469-12483, 1 June 1, 2021.
- [5] R. J. Reay, S. P. Kounaves and G. T. A. Kovacs, "An Integrated CMOS Potentiostat for Miniaturized Electroanalytical Instrumentation," *Proceedings of IEEE International Solid-State Circuits Conference*, San Francisco, CA, USA, 1994, pp. 162-163.
- [6] M. M. Ahmadi and G. A. Jullien, "Current-Mirror-Based Potentiostats for Three-Electrode Amperometric Electrochemical Sensors," in *IEEE Transactions on Circuits and Systems I: Regular Papers*, Vol. 56, no. 7, pp. 1339-1348, July 2009.
- [7] Bergveld, Piet. "The Impact of MOSFET-based Sensors." *Sensors and Actuators*, Vol. 8, no. 2 (1985): 109-127.
- [8] N. Moser, T. S. Lande, C. Toumazou and P. Georgiou, "ISFETs in CMOS and Emergent Trends in Instrumentation: A Review," in *IEEE Sensors Journal*, Vol. 16, no. 17, pp. 6496-6514, Sept. 1, 2016.
- [9] Decker, Eva L., and Ralf Reski. "Current Achievements in The Production of Complex Biopharmaceuticals with Moss Bioreactors." *Bioprocess and Biosystems Engineering*, Vol. 31, pp. 3-9, 2008.
- [10] Carlsson, Bengt. "An Introduction to Modeling of Bioreactors." *Systems and Control Group, Uppsala University, September*, Vol. 3, pp. 9, 1998.
- [11] Yuan, XiaoZi, Chaojie Song, Alison Platt, Nana Zhao, Haijiang Wang, Hui Li, Khalid Fatih, and Darren Jang. "A Review of All Vanadium Redox Flow Battery Durability: Degradation Mechanisms and Mitigation Strategies." *International Journal of Energy Research*, Vol. 43, no. 13, pp. 6599-6638, 2019.
- [12] Bozorgzadeh, Bardia, Daniel P. Covey, Christopher D. Howard, Paul A. Garris, and Pedram Mohseni. "A Neurochemical Pattern Generator SoC with Switched-electrode Management for Single-chip Electrical Stimulation and 9.3 μ W, 78 pArms, 400 V/s FSCV Sensing." *IEEE Journal of Solid-State Circuits*, Vol. 49, no. 4, pp. 881-895, 2014.
- [13] Sun, Alexander C., Enrique Alvarez-Fontecilla, A. G. Venkatesh, Eliah Aronoff-Spencer, and Drew A. Hall. "High-density Redox Amplified Coulostatic Discharge-based Biosensor Array." *IEEE Journal of Solid-State Circuits*, Vol. 53, no. 7, pp. 2054-2064, 2018.
- [14] Hickling, A. "Studies in electrode polarisation. Part IV. —The Automatic Control of The Potential of a Working Electrode." *Transactions of the Faraday Society*, Vol. 38, pp. 27-33, 1942.
- [15] Kissinger, Peter, and William R. Heineman, eds. *Laboratory Techniques in Electroanalytical Chemistry, Revised and Expanded*. CRC press, 2018.
- [16] Ahmadi, Mohammad M., and Graham A. Jullien. "A very low power CMOS potentiostat for bioimplantable applications." In *Fifth International Workshop on System-on-Chip for Real-Time Applications (IWSOC'05)*, pp. 184-189. IEEE, 2005.
- [17] Wang, Wei-Song, Wei-Ting Kuo, Hong-Yi Huang, and Ching-Hsing Luo. "Wide dynamic range CMOS potentiostat for amperometric chemical sensor." *Sensors*, Vol. 10, no. 3, pp. 1782-1797, 2010.
- [18] Liang, Yi-Fan, Chun-Yueh Huang, and Bin-Da Liu. "A voltammetry potentiostat design for large dynamic range current measurement." In *International Conference on Intelligent Computation and Bio-Medical Instrumentation*, pp. 260-263. IEEE, 2011.
- [19] Toprak, Serdar, Revna Acar Vural, and Okan Zafer Batur. "High accuracy potentiostat with wide dynamic range and linearity." *AEU-International Journal of Electronics and Communications*, Vol. 142, pp. 154018, 2021.
- [20] Bobacka, Johan, Ari Ivaska, and Andrzej Lewenstam. "Potentiometric ion sensors." *Chemical Reviews*, Vol. 108, no. 2, pp. 329-351, 2008.
- [21] Frank, Clyde. *Analytical chemistry*. Elsevier, 2012.
- [22] Zeng, Junming, Lei Kuang, Nicholas Miscourides, and Pantelis Georgiou. "A 128x128 current-mode ultra-high frame rate ISFET array with in-pixel calibration for real-time ion imaging." *IEEE Transactions on Biomedical Circuits and Systems*, Vol. 14, no. 2, pp. 359-372, 2020.
- [23] Miscourides, Nicholas, and Pantelis Georgiou. "Mismatch compensation in ISFET arrays using a parasitic programmable gate." In *2019 IEEE International Symposium on Circuits and Systems (ISCAS)*, pp. 1-5. IEEE, 2019.
- [24] Q. Lin *et al.*, "21.2 A 22 μ W Peak Power Multimodal Electrochemical Sensor Interface IC for Bioreactor Monitoring," *2023 IEEE International Solid-State Circuits Conference (ISSCC)*, San Francisco, CA, USA, 2023, pp. 314-316.
- [25] Liao, Yu-Te, Huanfen Yao, Andrew Lingley, Babak Parviz, and Brian P. Otis. "A 3 μ W CMOS Glucose Sensor for Wireless Contact-Lens Tear Glucose Monitoring." *IEEE Journal of Solid-State Circuits*, Vol. 47, no. 1, pp. 335-344, 2011.
- [26] Chung, Wen-Yaw, Arnold C. Paglinawan, Ying-Hsiang Wang, and Tsai-Tseng Kuo. "A 600 μ W readout circuit with potentiostat for amperometric chemical sensors and glucose meter applications." In *2007 IEEE Conference on Electron Devices and Solid-State Circuits*, pp. 1087-1090. IEEE, 2007.
- [27] Toumazou, Christofer, Leila M. Shepherd, Samuel C. Reed, Ginny I. Chen, Alpesh Patel, David M. Garner, Chan-Ju A. Wang *et al.* "Simultaneous DNA amplification and detection using a pH-sensing semiconductor system." *Nature Methods*, Vol. 10, no. 7, pp. 641-646, 2013.
- [28] Jung, Han Sae, Woo-Bin Jung, Jun Wang, Jeffrey Abbott, Adrian Horgan, Maxime Fournier, Henry Hinton *et al.* "CMOS electrochemical pH localizer-imager." *Science Advances*, Vol. 8, no. 30, 2022.
- [29] Huang, Yu-Jie, Te-Hsuen Tzeng, Tzu-Wei Lin, Che-Wei Huang, Pei-Wen Yen, Po-Hung Kuo, Chih-Ting Lin, and Shey-Shi Lu. "A self-powered CMOS reconfigurable multi-sensor SoC for biomedical

applications." *IEEE Journal of Solid-State Circuits*, Vol. 49, no. 4, pp. 851-866, 2014.

- [30] Laker, Kenneth R., and Willy MC Sansen. *Design of Analog Integrated Circuits and Systems*. Vol. 1. New York: McGraw-Hill, 1994.
- [31] Devices, Analog. "High Precision, Impedance, and Electrochemical Front End." *AD5940 Datasheet*, pp. 1-133, 2019.
- [32] Souza, Alexandre Kennedy Pinto, Carlos Augusto de Moraes Cruz, Greicy Costa Marques, Luis Smith Oliveira de Castro, and Thiago Brito Bezerra. "A compact current conveyor CMOS potentiostat circuit for electrochemical sensors." In *2019 4th International Symposium on Instrumentation Systems, Circuits and Transducers (INSCIT)*, pp. 1-6. IEEE, 2019.
- [33] Toprak, S., R. Acar Vural, and O. Zafer Batur. "Low Noise High Linearity Current Readout Topologies for Potentiostat Circuitry." In *2021 IEEE 32nd International Conference on Microelectronics (MIEL)*, pp. 219-222. IEEE, 2021.
- [34] Chan Carusone, Tony, D. Johns, and K. Martin. *Analog Integrated Circuit Design*. New York: Wiley.
- [35] Chin, Koken, Hao San, Atsushi Kitajima, Yoshiaki Arai, Jun Yamashita, and Hisashi Ito. "Leakage current compensation technique of ESD protection circuit for CMOS operational amplifier." In *2016 International Symposium on Intelligent Signal Processing and Communication Systems (ISPACS)*, pp. 1-4. IEEE, 2016.
- [36] Kang, Taewook, Inhee Lee, Sechang Oh, Taekwang Jang, Yejoong Kim, Hyochan Ahn, Gyouho Kim et al. "A 1.74. 12 mm 3 fully integrated pH sensor for implantable applications using differential sensing and drift-compensation." In *2019 Symposium on VLSI Circuits*, pp. C310-C311. IEEE, 2019.
- [37] Jarmin, R., Khuan Y. Lee, SF Mohammed Esa, H. Hashim, AZ Mohd Sih, and M. H. Abd Ghani. "ISFET characterization using constant voltage constant current readout circuit." *International Journal of Circuits, Systems and Signal Processing*, Vol. 9, pp. 47-53, 2015.
- [38] Hall, Drew A., Nagaraj Ananthapad Manabhan, Chulmin Choi, Le Zheng, Paul P. Pan, Carl W. Fuller, Pius P. Padayatti et al. "A CMOS Molecular Electronics Chip for Single-Molecule Biosensing." In *2022 IEEE International Solid-State Circuits Conference (ISSCC)*, Vol. 65, pp. 1-3. IEEE, 2022.
- [39] Chien, Jun-Chau, Hyongsok Tom Soh, and Amin Arbabian. "26.4 A Cell-Capacitance-Insensitive CMOS Sample-and-Hold Chronoamperometric Sensor for Real-Time Measurement of Small Molecule Drugs in Whole Blood." In *2020 IEEE International Solid-State Circuits Conference*, pp. 406-408. IEEE, 2020.
- [40] Manickam, Arun, Kae-Dyi You, Nicholas Wood, Lei Pei, Yang Liu, Rituraj Singh, Nader Gamini, Davood Shahrjerdi, Robert G. Kuimelis, and Arjang Hassibi. "11.2 A CMOS biosensor array with 1024 3-electrode voltammetry pixels and 93dB dynamic range." In *2019 IEEE International Solid-State Circuits Conference*, pp. 192-194. IEEE, 2019.
- [41] Jiang, Haowei, Xiahan Zhou, Saurabh Kulkarni, Michael Uranian, Rajesh Seenivasan, and Drew A. Hall. "A Sub-1 μ W multiparameter injectable BioMote for continuous alcohol monitoring." In *2018 IEEE Custom Integrated Circuits Conference (CICC)*, pp. 1-4. IEEE, 2018.
- [42] Lu, Shao-Yung, Siang-Sin Shan, Shih-Che Kuo, Cheng-Ze Shao, Yung-Hua Yeh, I-Te Lin, Shu-Ping Lin, and Yu-Te Liao. "18.4 A Wireless Multimodality System-on-a-Chip with Time-Based Resolution Scaling Technique for Chronic Wound Monitoring." In *2021 IEEE International Solid-State Circuits Conference (ISSCC)*, Vol. 64, pp. 282-284. IEEE, 2021.



currently working on sequencing chips.

Qiuyang Lin (S'16-M'20) received a M.S. in electrical engineering from Delft University of Technology in 2016 and a Ph.D. in biomedical integrated circuit design from Katholieke Universiteit Leuven, Belgium. Then, he continued as an Analog, Mixed-Signal R&D Design Engineer at IMEC in 2021. He is currently a senior researcher of Circuits & Systems for Health. He designed ASICs for wearable /ingestible applications such as electrocardiogram (ECG), bio-impedance (BIOZ) and photoplethysmography (PPG) readouts. He is the next-generation Electrochemical and DNA



electrocardiogram (ECG), bio-impedance (BIOZ) and photoplethysmography (PPG) readouts. Currently, his research is directed towards ingestibles, working on the next generation electrochemical Integrated Circuits (ICs) to be used in miniaturized wireless and ultra-low-power systems that can pass the gastrointestinal (GI) tract.

Wim Sijbers received the MS degree in electrical engineering from KU Leuven university in 2011. Since then, he has been working at imec as an analog design engineer. In 2017 he joined the Circuits and Systems for Health group as an analog design engineer. His work is focused on ultra-low power sensor interfaces for biomedical applications, more specifically for wearables and ingestibles. He worked on multiple analog and mixed signal Application Specific Integrated Circuits (ASICs) for vital sign monitoring, focusing on the front-ends for



biomedical sensing chips. Currently, she serves as an R&D Project Leader at imec, with focus on memory applications. Her interests involve biomedical readout circuits and Design Technology Co-Optimization (DTCO).

Christina Avdikou received her diploma in Electrical and Computer Engineering from Aristotle University of Thessaloniki (AUTH), Greece, in 2014, and she furthered her academic pursuits by obtaining a M.S. degree in Electrical Engineering with a focus on IC design from Katholieke Universiteit Leuven (KUL), Belgium, in 2016. From 2016 to 2020, she joined AnSem BV as an Analog and Mixed Signal IC Designer, working on industrial, automotive, and biomedical



projects. In 2020, she joined imec as a Researcher designing the next generation biomedical sensing chips. Currently, she serves as an R&D Project Leader at imec, with focus on memory applications. Her interests involve biomedical readout circuits and Design Technology Co-Optimization (DTCO).

Didac Gomez Salinas (M'17) received the B.S. and M.S. degrees in electrical engineering and the Ph.D. degree from Universitat Politècnica de Catalunya, Barcelona, Spain, in 2003, 2007, and 2013 respectively. From 2012 to 2016, he was with Broadcom, Spain as an analog designer. In 2016, he joined ICsense, Belgium working on custom ASICs design. In 2017 he joined IMEC to work in low power sensor interfaces. Since 2020 he is with Monolithic Power Systems working on mixed-signal circuits for power management.



the interception of imec's advanced semiconductor technology on future compute system challenges. He has authored several peer-reviewed journals,

Dwaipayan Biswas received the M.Sc. degree in system on chip and the Ph.D. degree in electrical engineering from University of Southampton (UoS), Southampton, U.K., in 2011 and 2015, respectively. From 2015 to 2016, he was a Postdoctoral Research Fellow with UoS. In 2016, he joined IMEC, as a researcher on digital IC design for biomedical applications. Currently he is leading a team of 10 researchers working on the System Technology Co-optimization (STCO) program at IMEC, Leuven, Belgium. His current research focusses on exploring

conferences, and edited a book. His research interests include low-power VLSI design, advanced technology for system optimization.



Bernardo Tacca received his M.Sc. degree in Microelectronics Engineering and his PhD degree in Space Systems and Technology from the University of Rome “Tor Vergata”, Rome, Italy. Previously, he worked as a Principal ASIC/FPGA Engineer for Airbus (Rome, Italy) and NXP Semiconductors (Eindhoven, The Netherlands) where he was responsible for the design, development, and verification of digital systems. He is currently a R&D Engineer at IMEC, Eindhoven, The Netherlands. His

research interests include VLSI design, FPGA programming, brain-machine interfacing, and signal processing for wireless communications.



Nick Van Helleputte (M'07) received the MS degree in electrical engineering in 2004 from the Katholieke Universiteit Leuven, Belgium. He received his Ph.D. degree from the same institute in 2009 (MICAS research group). His PhD research focused on low-power ultra-wide-band analog front-end receivers for ranging applications. He joined imec in 2009 as an Analog R&D Design Engineer. He is currently Scientific director of Circuits & Systems for health. His research focus is on ultra-low-power circuits for biomedical applications. He has been involved in analog and

mixed-signal ASIC design for wearable and implantable healthcare applications. Nick is an IEEE and SSCS member (SSCS Distinguished Lecturer '17-'18) and served on the technical program committee of VLSI circuits symposium and ISSCC. Since 2020, he is also associated editor for the IEEE Journal of Solid-State Circuits.